Full paper

Polarization-free high-crystallization β-PVDF piezoelectric nanogenerator toward self-powered 3D acceleration sensor

Long Jin[a,1], Songyuan Ma[a,1], Weili Deng[a], Cheng Yan[a], Tao Yang[a], Xiang Chu[a], Guo Tian[a], Da Xiong[a], Jun Lu[a,*], Weiqing Yang[a,b,*,2]

[a] *Key Laboratory of Advanced Technologies of Materials (Ministry of Education), School of Materials Science and Engineering, Southwest Jiaotong University, Chengdu 610031, PR China*
[b] *State Key Laboratory of Traction Power, Southwest Jiaotong University, Chengdu 610031, PR China*

A B S T R A C T

The strong piezoelectric lead zirconate titanate (PZT) ceramic with inherent brittleness and highly tough Poly (vinylidene fluoride) (PVDF) polymer with intrinsic weak piezoelectricity cannot simultaneously fulfill the requirements of high sensitivity and excellent stability as a piezoelectric acceleration sensor in extreme service environments, such as intense impact. Here, we developed a polarization-free high-crystallization β-PVDF (hβ-PVDF) based piezoelectric nanogenerator (PENG) as acceleration sensor with high sensitivity ($2.405\ \mathrm{nA\ s^2\ m^{-1}}$) and excellent stability (97% remaining after 10000 cycles). Fundamentally, the excellent performance benefits from the PVDF by high-pressure melt crystallization with a high β-phase crystallinity of 86.48%, indicative of the enhanced piezoelectricity (high short-circuit current density of $145\ \mathrm{nA\ cm^{-2}}$). With integration of PENGs in three axes, the self-powered 3D acceleration sensor is developed for vector acceleration measurement in any directions. Moreover, a dynamic 3D frequency and acceleration sensor system is targetedly applied to cooperate the acceleration sensor for real-time collision monitoring and alert signal transmission, which presents a significant step toward vehicle safety monitoring. Therefore, we believe this easy process of hβ-PVDF and device has potential for commercial production in the field of transportation, self-powered devices, and energy harvesting.

1. Introduction

Piezoelectric acceleration sensor plays a crucial and essential role in many fields, such as large mechanical structure testing [1], national defense, transportation [2], auto industry [3], biomedical devices [4], and so on. Usually, commercial piezoelectric acceleration sensor is made by ceramic [5,6], such as lead zirconate titanate (PZT), owing to its eminent piezoelectric performance [7–9]. However, the application of piezoelectric ceramic acceleration sensors is largely limited in intense impact, high shear force, and other extreme service environments, because of the inherent brittleness performance [10,11]. What's more, the polarization with an energy-intensive [12] and complex process is indispensable to PZT [10,13]. Besides, Poly (vinylidene fluoride) (PVDF), representative piezoelectric polymer, is another good choice for its excellent impact resistance and toughness [14–17]. Unfortunately, the piezoelectric performance is not strong enough [18–20], leading to low sensitivity for sensors. Herein, applying

polarization-free, piezoelectricity-enhanced PVDF for high sensitivity acceleration sensor to fulfill the harsh requirement of intense impact is mandatory and desirable.

Piezoelectric nanogenerator (PENG) was first proposed in 2006 for energy conversion in nanoscale [21]. Nowadays, PENG based on PVDF has attracted adequate attention [22–26] owing to its flexibility, high durability, as well as biodegradability. As we know, the piezoelectricity of PVDF-based PENG mainly originated from β-phase PVDF [20,27–29] and additionally expensive post-polarization [30]. Although this PVDF could assuredly meet requirement of mechanical stability during extreme service environments such as intense impact, its relatively lower piezoelectricity due to low β-phase crystallinity [31–33] and piezoelectric stability [34] due to inevitable depolarization of post-polarization intrinsically hinder the further commercial applications of PVDF-based PENG.

In this work, we present a novel polarization-free high-crystallization β-PVDF (hβ-PVDF) based PENG as self-powered acceleration

---

sensor. This hβ-PVDF by high-pressure melt crystallization amazingly presents an intrinsic crystallinity of β-phase as high as 86.48%, which is beneficial to high and steady piezoelectricity of PENG. What's more, the structure of nanosheets is formed during the preparation, exhibiting piezoelectricity enhancement (short-circuit current density can reach up to 145 nA cm^{-2}). At an external acceleration ranging from 5 m/s^2 to 30 m/s^2, the fabricated sensor shows extremely linear relationship between the output current and the acceleration, with a high sensitivity of 2.405 nA s^2 m^{-1}, demonstrative of the good performance as an acceleration sensor. Under a frequency of 4 Hz, the short-circuit current of PENG still remains 97% after 10000 cycles, evidently revealing the excellent robustness. Integrated with three PENGs, the self-powered 3D acceleration sensor is developed for vector acceleration measurement in any directions, as well as the compositions in three axes respectively. In addition, a real-time 3D frequency and acceleration sensor system is developed for vehicle monitoring system to avoid casualties when there is a vehicle accident. This provides experienced reference on solving problems in vehicle safety monitoring and automobile security system. In prospect, the easy process of hβ-PVDF and the high sensitivity device provides potential for commercial production in many fields, such as transportation, self-powered devices, energy harvesting and so on.

2. Results and discussion

Fig. 1a schematically shows the device structure of self-powered 3D acceleration sensor, consisting of three component PENGs, and its photograph is also presented in Fig. 1b. As illustrated in Fig. 1c, the PENG, as 1D sensor, can be divided into two parts, mover and stator. The mover is a cylinder mass connected with two acrylic disks through two springs. There are two hβ-PVDF slices with aluminum electrodes on both sides as stators. Finally, they are packaged into an acrylic tube

with two acrylic substrates. This ingenious design enable the springs to store external energy for compressing hβ-PVDF, resulting electronic output due to piezoelectricity. It is worth mentioning that the excellent piezoelectricity is attributed to the preparation process of hβ-PVDF. The detailed process is presented in Fig. 1d. First, raw materials of PVDF is put into a self-made piston-cylinder. Then temperature is increased and pressure is applied, resulting nano structure in this process. Detailedly, the scanning electron microscope (SEM) image of the nanosheets in Fig. 1e reveals the key to piezoelectricity. Finally the hβ-PVDF slice is completed after cooling down to ambient conditions. It is precisely because of the high pressure and high temperature situations, the prepared PVDF has higher crystallinity of sample and β-phase, exhibiting better piezoelectricity.

The comprehensive and systematic demonstrations of hβ-PVDF play a vital role to further exploit the advantages of its advantages for the accurate development of PENG-based 3D acceleration sensor. To begin with, crystal property characterizations of PVDF with different process methods are employed in Fig. 2. According to differential scanning calorimetry (DSC), shown in Fig. 2a, the area of the melting peaks changes with the process methods changing, comfortably indicating more crystallites formed in the high-pressure and high-temperature treated sample. Furthermore, the melting point turns to shift to higher when the sample is processed with high pressure and high temperature, while the samples with atmospheric pressure and solution method have a lower value. This suggests alterations of crystalline forms, morphologies and substructures, owing to the process of high pressure. Wide-angle X-ray diffraction (WAXD) and attenuated total reflectance Fourier transform infrared spectroscopy (ATR-FTIR) were used for identification of crystalline phases, further confirming a sharp increase in the ratio of β-phase, when the process of high temperature and high pressure was applied. In Fig. 1b and c, it can be evidently observed by the
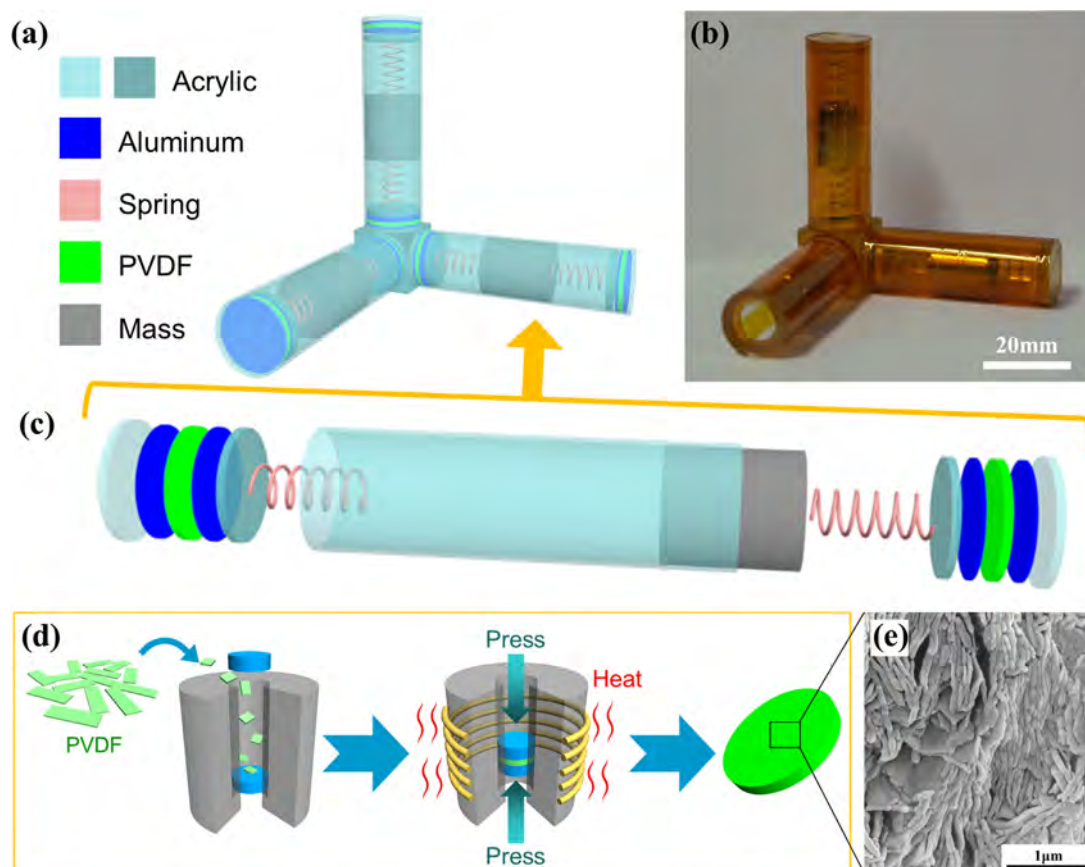

Fig. 1. Device structure of self-powered 3D acceleration sensor. (a) Schematic diagram and (b) photograph of the as-fabricated sensor. (c) The detailed structural composition of 1D sensor. (d) The preparation process of hβ-PVDF in a piston-cylinder high pressure apparatus. (e) SEM image of nanosheets of hβ-PVDF.
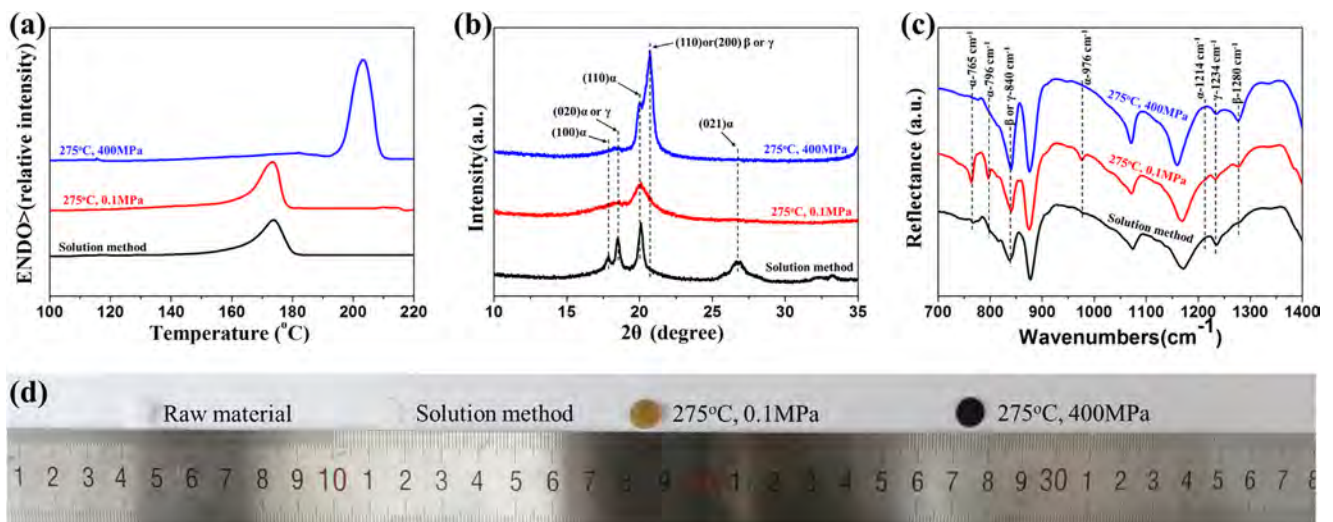
Fig. 2. Crystal property characterizations. (a) DSC, (b) WAXD, and (c) ATR-FTIR results of PVDF samples with different preparation methods. (d) Photograph of raw material and samples of different process methods.
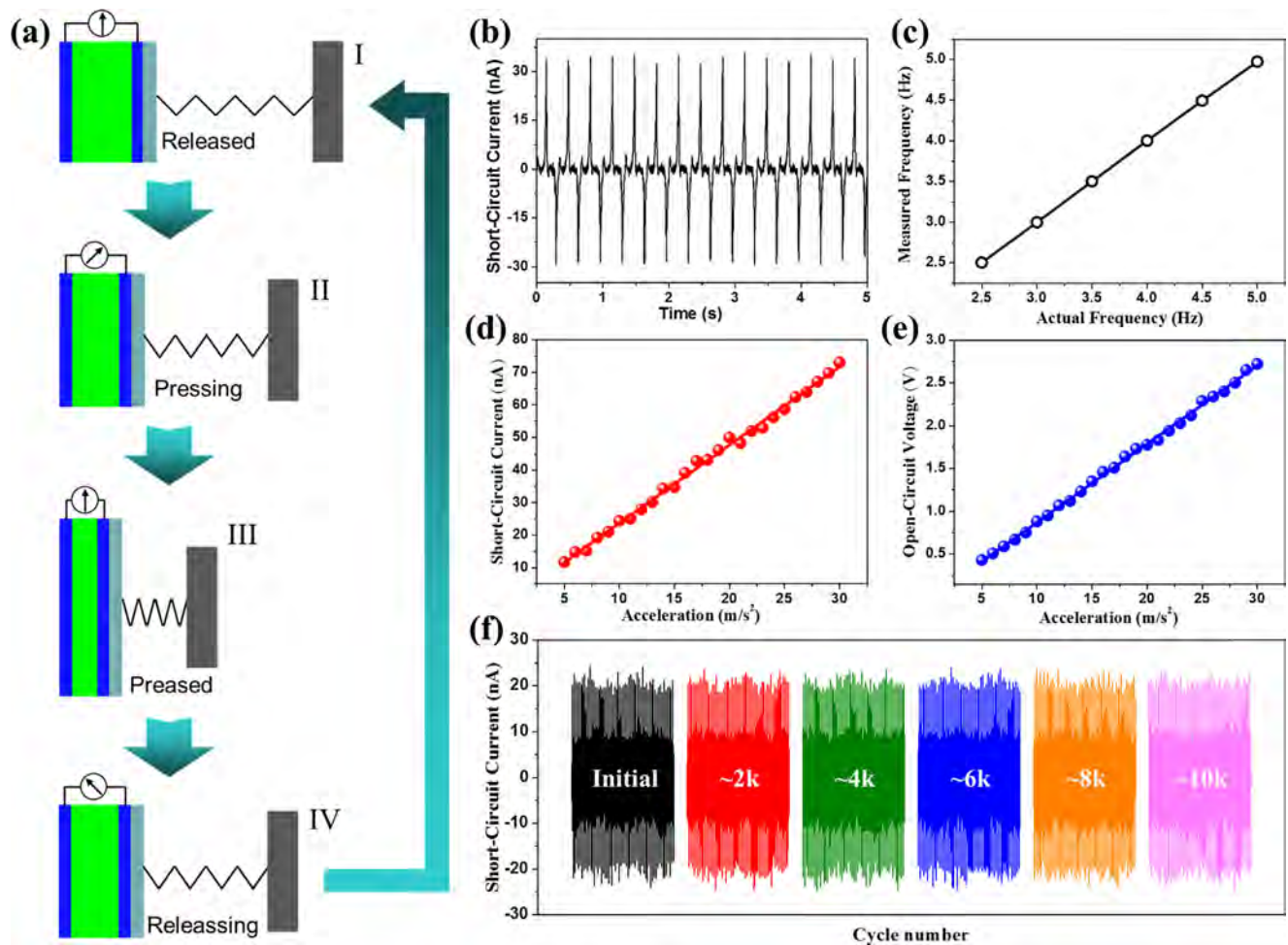

Fig. 3. Working principle and electrical property of the acceleration sensor. (a) Schematic diagram showing the basic working principle of electricity generation by hβ-PVDF. (b) The typical waveform of short-circuit current for acceleration and frequency analysis at 3 Hz. (c) Measured frequency (abstracted from fast Fourier transform (FFT)) over different actual frequency. Dependence of the (d) short-circuit current and (e) open-circuit voltage with different acceleration ranging from 5 m/s^2 to 30 m/s^2. (f) Stability and durability test under 10 m/s^2 for about 10000 cycles.

intensity variation of the apparent single peak at 2θ angle 20.4–21.1°, from the superposition of the (110) β and (200) β reflections (WAXD), corresponding to the bands at 840 and 1280 cm^{-1} (ATR-FTIR), which is characteristic of piezoelectric β-phase of PVDF [30,35,36]. Though the intensities of characteristic reflections are relatively weaker, especially in the high-pressure treated sample, other negligible crystalline forms, such as α and γ phase, can be also detected. Compared with other methods, high-pressure crystallization leads to higher crystallinity of sample and β-phase simultaneously (the detailed results can be seen in Table S1). Fig. 2d presents the raw materials and samples of different process methods.

To elucidate the working principle of the acceleration sensor, both COMSOL simulation (Fig. S1) and two-dimensional schematic diagram have been taken. Fig. 3a describes the electricity generation process. First, the spring is released, causing no external force on the hβ-PVDF, which is the initial state. Thus, there is a balance between the dipole moment and electrode, leading to the absence of any charge flowing, and no current occurs. Then, when there is vibration, the mass moves and presses the spring, owing to the inertia. In this process, the external energy is stored in the spring, and there is force on the hβ-PVDF, resulting in the piezoelectric potential. As a result, negative charges are generated on the right side, and the positive charges on the left side. To balance it, positive and negative charges are induced on the right and left electrodes through external circuit, respectively, leading to a generation of voltage and current. On the next state, the spring is fully pressed. In other words, the energy stored in the spring has reached maximum. This is a new balance, in which there is no charge flows and the voltage reaches peak value. Subsequently, the mass moves oppositely, and the spring starts to release the energy stored previously, resulting in reduced force on the hβ-PVDF. In this process, the dipole moment is returning to its original value, and the induced charges flow back to the reverse direction. As a result, an electric signal is detected again between the right and left electrodes. Finally, the mass moves to the original position and the spring get released again, the same as original state, completing a whole cycle of electricity generation. In

short, the vibration force produces alternating current signal, because of the piezoelectricity of hβ-PVDF.

To characterize the performance of the sensor for acceleration, the electrical output property has been measured. For quantitative measurement, the sensor was fixed on a programmable linear motor, moving simultaneously with it. Fig. 3b shows a typical waveform of short-circuit current, as a basis for further frequency analysis and acceleration calculation. Frequency is conducted by fast Fourier transform (FFT) at actual frequency of 2.5–5 Hz (Fig. S2), and the result exhibits a strong linear relationship between actual and measured frequency, confirming it as a sensor for frequency measurement. As can be seen in Fig. S3, the amplitude of short-circuit current and open-circuit voltage increase almost linearly with the increased acceleration ranging from 5 to 30 m/s^2. The values of short-circuit current is drawn in Fig. 3d, and fitted into a line with a correlation coefficient of 0.996 and a slope of 2.405. It suggests that the acceleration sensor has a high sensitivity of 2.405 nA s^2 m^{-1} (calculated in Supporting information), which is beneficial for practical applications. At 30 m/s^2, the short-circuit current density can reach up to 145 nA cm^{-2} (calculated in Supporting information). The dependence of open-circuit voltage and acceleration has been also invested in Fig. 3e, indicating linear relation. Finally, the short-circuit current signals with a remaining 97% after about 10000 cycles under 4 Hz point out the excellent stability and durability of the acceleration sensor, as shown in Fig. 3f. Therefore, these tests definitively prove the sensor for acceleration and frequency measurement, by processing the short-circuit current.

On basis of three 1D sensors, the 3D vector acceleration sensor is developed, and the characteristics of dimensional acceleration are exhibited in Fig. 4. When the 3D acceleration sensor is fixed to a certain axis, in which there is external acceleration, for example X axis, the hβ-PVDF in the 1D sensor subjected along X axis can be only pressed. Meanwhile, there is no pressure on the hβ-PVDF in the other axes. Fig. S4a shows the test model, and Fig. S4b is the enlarged view of supporting base. Measured current and calculated acceleration of X axis, Y axis and Z axis are detailedly shown in Fig. S4c-h. Similar with the one
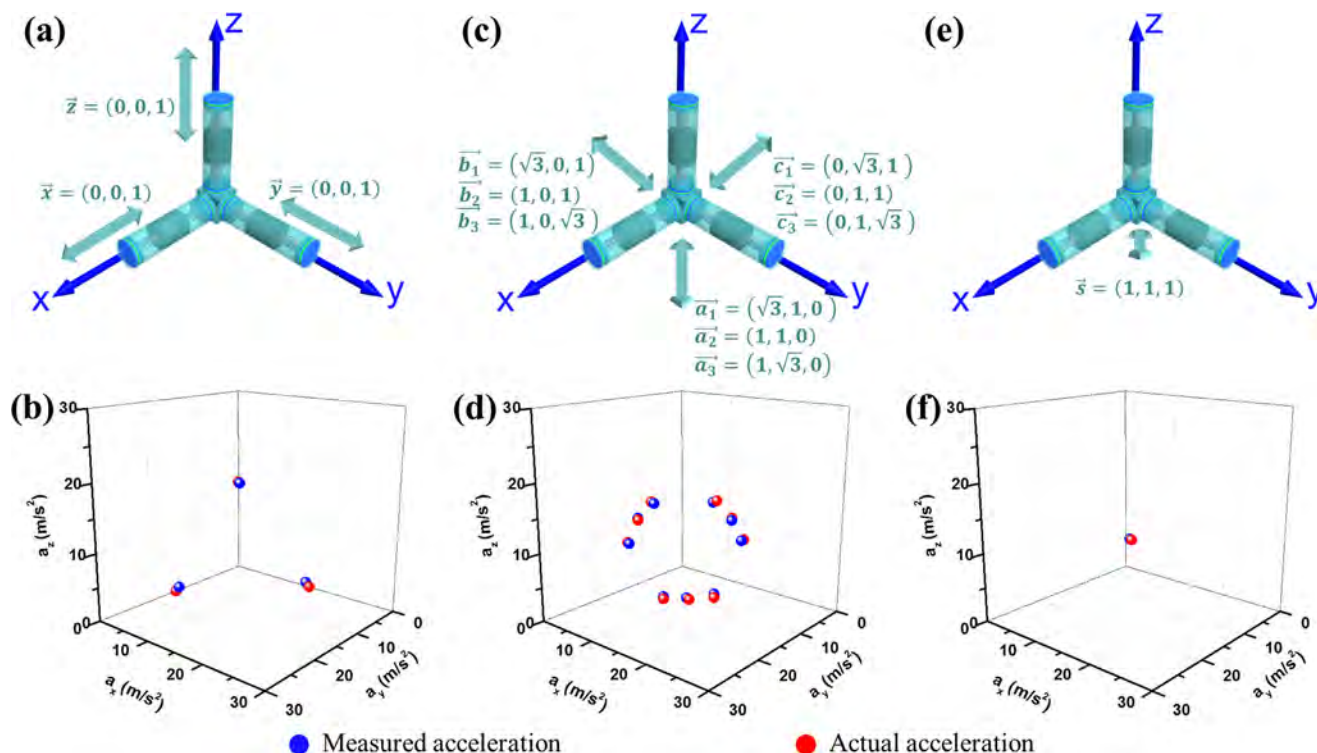

Fig. 4. Characteristic study of the vector acceleration in three dimension. The external vector acceleration and the measured vector acceleration (a, b) along one axis, (c, d) on one coordinate plane, and (e, f) in three dimension space at an external of acceleration of 15 m/s^2.
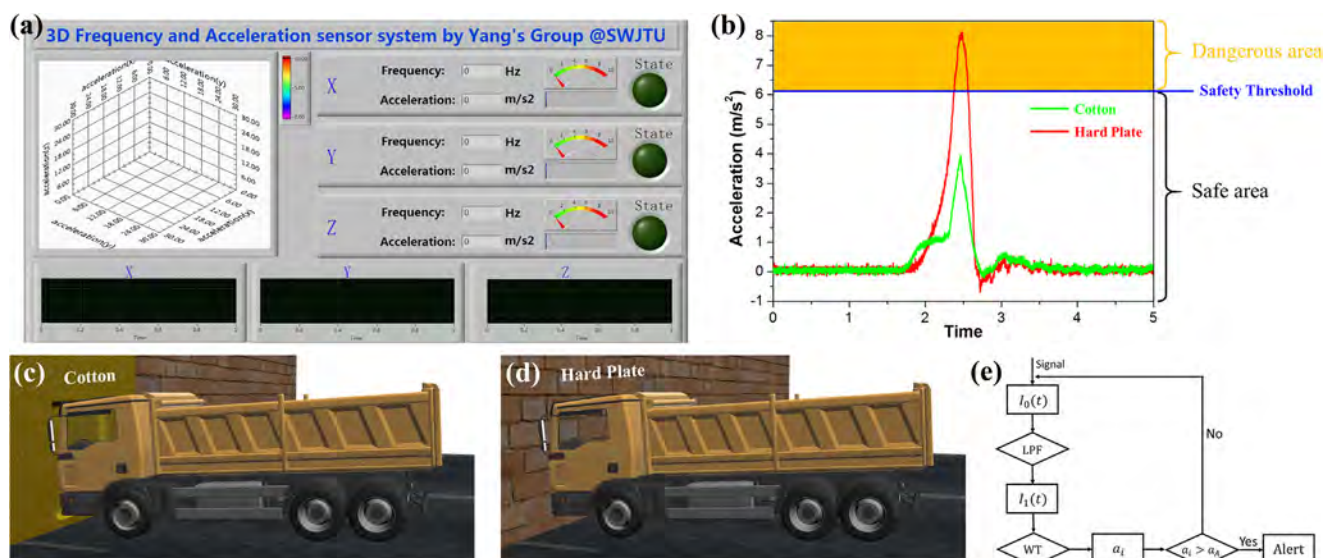
Fig. 5. The application of 3D acceleration sensor in dynamic vehicle monitoring system. (a) Dynamic 3D frequency and acceleration monitoring system interface. (b) The monitoring data from 3D acceleration sensor in a truck model. Schematic diagram of vehicle collision with (c) cotton and (d) hard plate. (e) System algorithm flow chart.

subjected to a certain axis, Figs. S5 and S6 show the cases when the 3D acceleration sensor is subjected on one coordinate plane, including directions of 30°, 45° and 60°. Furthermore, the case in three dimension space has been also investigated in Fig. S7, leading to a good performance. In the test process, a key step is to choose an applicable supporting base, and the test videos can be seen in Movie 1, 2, 3 and 4. At external acceleration of 15 m/s², the measured and actual acceleration are compared in the same coordinate system, as indicated in Fig. 4. The blue points represent the measured acceleration while the red points represent the actual acceleration. It is obvious that the measured accelerations accord approximately with the actual accelerations, in which the maximum relative error is only 4%. Besides, the deviation angles are also calculated in Supporting information, demonstrating the great accuracy of 3D acceleration sensor. In brief, the experimental results demonstrate the correctness and affectivity of the 3D sensor for vector acceleration measurement in any directions. The detailed data are shown in Table S2. On the other hand, it is proved to be an energy harvester to charge a capacitor, shown in Fig. S9.

Supplementary material related to this article can be found online at http://dx.doi.org/10.1016/j.nanoen.2018.05.068.

To prove the 3D acceleration sensor practical in the applications, a point-by-point version of the procedure is implemented by LabVIEW. Fig. 5a displays the interface of 3D frequency and acceleration sensor system, including frequency sensing, acceleration sensing and state alert in each axis. In addition, the dynamic coordinate system can reveal the vector acceleration in time. As application, a vehicle collision is simulated to demonstrate the 3D acceleration sensor in the vehicle collision safety system. When a vehicle collision with cotton takes place, the system has no alert, as shown in Fig. S8a and movie 5. As for the reason, it is because the impact force is below the pre-set safety threshold, causing no danger to human. The measured data is concretely presented in Fig. 5b. The orange area beyond safety threshold is dangerous area, and the below white area is safe, offering a judgment of danger. When a vehicle collision with hard plate, the alert is triggered immediately (Fig. S8b and Movie 6). This helps the safety air bag to be triggered for human life protection. As can be seen in Fig. 5b, the peak of red curve is beyond safety threshold, indicating the dangerous condition while the green curve is below the safety threshold. Fig. 5c and d schematically illustrate the vehicle collision with cotton and hard plate, respectively. Fig. 5e shows the algorithm flow chart. Based on the novel sensor, low-pass filter (LPF) is used to process the signals acquired for

filtering the environmental noise, and then the signals is calculated by wavelet transformation (WT) to get the amplitude, corresponding to the measured acceleration. Finally the judgment command is proposed to select alert or not. As a consequence, the 3D acceleration sensor can monitor the safety state in the vehicle safety system, and has potential application in the automobile security system.

Supplementary material related to this article can be found online at http://dx.doi.org/10.1016/j.nanoen.2018.05.068.

3. Conclusion

In summary, a self-powered acceleration sensor based on polarization-free hβ-PVDF PENGs was developed. For as-prepared PENG-based sensor, the relationship between short-circuit current and acceleration was investigated ranging from 5 m/s² to 30 m/s² with an excellently linear sensitivity of 2.405 nA s² m⁻¹. What's more, the output current of PENG-based sensor has a remarkable robustness of remaining 97% after 10000 cycles under 4 Hz. Therefore, this self-powered acceleration sensor can simultaneously fulfill the requirements of high sensitivity and excellent stability. Also, frequency can be measured by processing the signals. More importantly, consisting of three component PENGs, the fabricated 3D sensor can measure vector acceleration in any directions with minor errors. Finally, a dynamic 3D frequency and acceleration sensor system is developed, fully demonstrating the applicability, especially in vehicle safety system. This work not only provides an effective experienced reference on solving problems in vehicle safety system, but also dramatically expands PENG's application in self-powered fields.

4. Experimental section

4.1. Preparation of hβ-PVDF

The sample of solution method was prepared with PVDF raw materials and N, N-dimethylformamide (DMF). Put PVDF raw materials and DMF into a glass container and then stir them at 60 °C for 5 h. Finally, the mixed solution was coated on glass substrates at 80 °C for 3 h to remove the DMF solvent, and the sample of solution method was gotten. Put PVDF raw materials into a self-made piston-cylinder, and increase the temperature to 200 °C to allow them to melt. Then apply a low pressure of 150 MPa and raise the temperature to 275 °C. After

equilibrium was established, the pressure was further adjusted to 400 MPa. 10 min later, quench down to ambient conditions. Thus, the sample of high temperature and high pressure was gotten. With respect to the sample of high temperature and atmospheric pressure, after the process of melting PVDF raw materials, apply normal pressure and 275 °C for 10 min. Finally quench down to ambient conditions, the sample was prepared. The prepared sample has a thickness of 660 μm and radius of 4 mm.

4.2. Fabrication of the device

The device can be separated into three PENGs and a supporting base. The supporting base was six acrylic plates stuck together as a cube. The PENG was fabricated simply. First, an iron cylinder mass was connected with two acrylic disks through two springs by glue. It can be regarded as a mover. Then, two hβ-PVDF samples were adhered with aluminum foil on both sides as stators. Next, the mover and stators were put into an acrylic tube. Finally, use two acrylic substrates to package the tube. Thus, a PENG was finished. Adhering three PENGs to three sides of the supporting base makes a fabricated device.

4.3. Materials characteristics

A NTIAG HS01-37 × 166 linear motor was used as impact source. DSC measurement was conducted at atmospheric pressure by a TA-Q20 instrument. WAXD results were obtained with a DX-1000 diffractometer. ATR-FTIR data was obtained with a Nicolet 5700 spectrometer. Microstructure of hβ-PVDF images were obtained from SEM (FEI QUANTA FEG 250). Before test, there is a pretreatment. First, add 30 g P_2O_5, 60 ml H_2SO_4 (98%) and 0.3 g Cr_2O_3 into a beaker as etching liquid, and heat it to 90 °C. Then, put the sample into the etching liquid and keep 90 °C for 20 h. Finally, wash it by deionized water for 5 times. We can get the sample for SEM.

4.4. Measurement of electric performance

The output voltage signals were measured by a low-noise voltage preamplifier (Keithley 6514 system electrometer). The output current voltage signals were measured by a low-noise current preamplifier (Stanford Research SR570).

Acknowledgments

Author contributions

Long Jin and Songyuan Ma contributed equally to this work.

Notes

The authors declare no competing financial interest.

Appendix A. Supporting information

Supplementary data associated with this article can be found in the online version at http://dx.doi.org/10.1016/j.nanoen.2018.05.068.

References

[1] H. Yu, X. He, W. Ding, Y. Hu, D. Yang, S. Lu, C. Wu, H. Zou, R. Liu, C. Lu, Z.L. Wang, Adv. Energy Mater. 7 (2017) 1700565.

[2] Y.K. Pang, X.H. Li, M.X. Chen, C.B. Han, C. Zhang, Z.L. Wang, ACS Appl. Mater. Interfaces 7 (2015) 19076–19082.

[3] J. Hillenbrand, M. Kodejska, Y. Garcin, H.V. Seggern, IEEE Trans. Dielectr. Electr. Insul. 17 (2010) 1021–1027.

[4] B. Zhang, L. Zhang, W. Deng, L. Jin, F. Chun, H. Pan, B. Gu, H. Zhang, Z. Lv, W. Yang, Z.L. Wang, ACS Nano 11 (2017) 7440–7446.

[5] Y. Hu, Z.L. Wang, Nano Energy 14 (2015) 3–14.

[6] S. Patrick, G. Jens Ole, K. Lars Munch, J. Micromech. Microeng. 6 (1996) 131.

[7] G. Tang, B. Yang, C. Hou, G. Li, J. Liu, X. Chen, C. Yang, Sci. Rep. 6 (2016) 38798.

[8] C. Dagdeviren, Y. Shi, P. Joe, R. Ghaffari, G. Balooch, K. Usgaonkar, O. Gur, P.L. Tran, J.R. Crosby, M. Meyer, Y. Su, R. Chad Webb, A.S. Tedesco, M.J. Slepian, Y. Huang, J.A. Rogers, Nat. Mater. 14 (2015) 728–736.

[9] M. Sobocinski, M. Leinonen, J. Juuti, N. Mantyniemi, H. Jantunen, Sens. Actuators, A 216 (2014) 370–375.

[10] K.I. Park, J.H. Son, G.T. Hwang, C.K. Jeong, J. Ryu, M. Koo, I. Choi, S.H. Lee, M. Byun, Z.L. Wang, K.J. Lee, Adv. Mater. 26 (2014) 2514–2520.

[11] A.M. Roji M, J.G., A.B. Raj T, RSC Adv. 7 (2017) 33642–33670.

[12] W. Deng, L. Jin, B. Zhang, Y. Chen, L. Mao, H. Zhang, W. Yang, Nanoscale 8 (2016) 16302–16306.

[13] S.R. Anton, H.A. Sodano, Smart Mater. Struct. 16 (2007) R1–R21.

[14] X. Chen, X. Han, Q.-D. Shen, Adv. Electron. Mater. 3 (2017) 1600460.

[15] X. Shuai, P. Zhu, W. Zeng, Y. Hu, X. Liang, Y. Zhang, R. Sun, C.P. Wong, ACS Appl. Mater. Interfaces 9 (2017) 26314–26324.

[16] R.I. Haque, R. Vié, M. Germainy, L. Valbin, P. Benaben, X. Boddaert, Flex. Print. Electron. 1 (2016) 015001.

[17] A. Gaur, C. Kumar, R. Shukla, P. Maiti, ChemistrySelect 2 (2017) 8278–8287.

[18] C. Sun, J. Shi, D.J. Bayerl, X. Wang, Energy Environ. Sci. 4 (2011) 4508.

[19] N.A. Hoque, P. Thakur, S. Roy, A. Kool, B. Bagchi, P. Biswas, M.M. Saikh, F. Khatun, S. Das, P.P. Ray, ACS Appl. Mater. Interfaces 9 (2017) 23048–23059.

[20] N.R. Alluri, A. Chandrasekhar, J.H. Jeong, S.-J. Kim, J. Mater. Chem. C 5 (2017) 4833–4844.

[21] Z.L. Wang, J.H. Song, Science 312 (2006) 242–246.

[22] M. Han, X. Chen, B. Yu, H. Zhang, Adv. Electron. Mater. 1 (2015) 1500187.

[23] Y. Mao, P. Zhao, G. McConohy, H. Yang, Y. Tong, X. Wang, Adv. Energy Mater. 4 (2014) 1301624.

[24] S. Siddiqui, H.B. Lee, D.-I. Kim, L.T. Duy, A. Hanif, N.-E. Lee, Adv. Energy Mater. 8 (2017) 1701520.

[25] Y. Zi, L. Lin, J. Wang, S. Wang, J. Chen, X. Fan, P.K. Yang, F. Yi, Z.L. Wang, Adv. Mater. 27 (2015) 2340–2347.

[26] L. Persano, C. Dagdeviren, Y. Su, Y. Zhang, S. Girardo, D. Pisignano, Y. Huang, J.A. Rogers, Nat. Commun. 4 (2013) 1633.

[27] N. Soin, P. Zhao, K. Prashanthi, J. Chen, P. Ding, E. Zhou, T. Shah, S.C. Ray, C. Tsonos, T. Thundat, E. Siores, J. Luo, Nano Energy 30 (2016) 470–480.

[28] S.K. Karan, D. Mandal, B.B. Khatua, Nanoscale 7 (2015) 10655–10666.

[29] Y. Wada, R. Hayakawa, Ferroelectrics 32 (1981) 115–118.

[30] C. Xu, L. Zhang, Y. Xu, Z. Yin, Q. Chen, S. Ma, H. Zhang, R. Huang, C. Zhang, L. Jin, W. Yang, J. Lu, J. Mater. Chem. A 5 (2017) 189–200.

[31] A. Gheibi, R. Bagherzadeh, A.A. Merati, M. Latifi, J. Polym. Res. 21 (2014) 571.

[32] C. Ribeiro, V. Sencadas, J.L.G. Ribelles, S. Lanceros-Méndez, Soft Mater. 8 (2010) 274–287.

[33] H.H. Singh, S. Singh, N. Khare, Polym. Adv. Technol. 29 (2018) 143–150.

[34] S. Siddiqui, D.-I. Kim, E. Roh, L.T. Duy, T.Q. Trung, M.T. Nguyen, N.-E. Lee, Nano Energy 30 (2016) 434–442.

[35] D. Zhang, P. Tian, X. Chen, J. Lu, Z. Zhou, X. Fan, R. Huang, Compos. Sci. Technol. 77 (2013) 29–36.

[36] C. Lu, L. Zhang, C. Xu, Z. Yin, S. Zhou, J. Wang, R. Huang, X. Zhou, C. Zhang, W. Yang, J. Lu, RSC Adv. 6 (2016) 67400–67408.

Long Jin received his B.E. from Southwest Jiaotong University in 2015. He is currently pursuing Ph.D. degree in materials science and engineering at Southwest Jiaotong University.

Songyuan Ma received his B.S. degree in Material Science and Engineering from Tianjin Polytechnic University (TJPU), in China. He is now a master candidate in Materials Engineering at Southwest Jiaotong University (SWJTU). His research interest includes phase transition and piezoelectric properties of hybrid composites crystallized at high pressure

Guo Tian, as a junior student of Southwest Jiaotong University (SWJTU) of China, majors in Materials Science and Engineering, and he will pursue his master degree in next three years in SWJTU.

Weili Deng received his B.S. degree in electronic science and technology from Chongqing University in 2006, and then earns his master degree in 2009. Now he is a doctor in materials science and engineering at Southwest Jiaotong University.

Da Xiong is a college student in Southwest Jiaotong University of China. He majors in Materials Science and Engineering. His recent research focus on nanogenerators and flexible optoelectronic device.

Cheng Yan received his B.S. from Southwest Jiaotong University in 2017. He is currently pursuing Ph.D. degree in materials science and engineering at Southwest Jiaotong University. His research focuses on the flexible electronics and self-powered sensors.

Jun Lu, other used names Jun Lyu and Jun Lv, received his bachelor degree in polymer engineering from Harbin Institute of Technology, China in 1992, and PhD degree in material processing engineering from Sichuan University, China in 2006. He worked respectively as a postdoctoral fellow and senior researcher at Chonnam National University, South Korea from 2006 to 2008. He joined Southwest Jiaotong University, China as an associate professor in 2008, and then got promoted to full professor in 2014. His current research focuses on processing and properties of advanced functional polymeric materials and their optoelectronic devices.

Tao Yang received his B.S. in materials science and engineering from Southwest Jiaotong University in 2017. He is currently pursuing master's degree in materials science and engineering at Southwest Jiaotong University. His research focuses on the flexible electronics and self-powered sensors.

Weiqing Yang received his M.S. in Physics in 2007, and Ph.D. in Materials Science and Engineering from Sichuan University in 2011. He was a post-doctorate research fellow at University of Electronic Science and Technology of China from 2011 to 2013. Subsequently, he was a post-doctorate research fellow at Georgia Institute of Technology from 2013 to 2014, under the supervision of Prof. Zhong Lin Wang. His main research interest includes energy harvesting and storage devices, such as supercapacitors and nanogenerators

Xiang Chu received his B.S. degree in Materials Science and Engineering from Southwest Jiaotong University (SWJTU), PR China in 2016. He is now a master candidate in Materials Science and Engineering at SWJTU. His research interest includes nano-materials for electrochemical energy storage devices.